On Oscillatory Instability of Convective Flows at Low Prandtl Number

A. Yu. Gelfgat
Research Associate.
Mem. ASME

P. Z. Bar-Yoseph
Professor.
Mem. ASME

A. L. Yarin
Professor.

Computational Mechanics Laboratory,
Faculty of Mechanical Engineering,
Technion-Israel Institute of Technology,
Haifa 32000, Israel

Numerical investigation of the oscillatory instability of convective flows in laterally heated rectangular cavities is presented. Cavities with no-slip isothermal vertical boundaries, no-slip adiabatic lower boundary, and stress-free adiabatic upper boundary are considered. Dependence of the critical Grashof number and the critical frequency of oscillations on the aspect ratio (A = length/height) of the cavity are investigated. The stability diagrams were obtained for the whole interval of the aspect ratio $1 \le A \le 10$. The study was carried out for two values of the Prandtl number, $Pr = 0$ and 0.015. It was shown that the oscillatory instability sets in as a result of the Hopf bifurcation. It was found that at two different values of the Prandtl number considered the instability is caused by different infinitely small dominant perturbations, which means that the convective heat transfer strongly affects stability of the flow even for cases having small Prandtl number. No asymptotic behavior for large aspect ratios was found up to $A = 10$. Slightly supercritical oscillatory flows were approximated asymptotically by means of the weakly nonlinear analysis of the calculated bifurcation.

Introduction

The present study is devoted to numerical analysis of the transition from steady to oscillatory state of convective flows at low-Prandtl-number in a laterally heated rectangular cavity. This problem attracted a wide scientific interest after experiments of Hurle et al. (1974) showed that convective oscillations cause lattice structure of a growing crystal in the processes of crystal growth from a liquid phase. A particular case of a cavity with aspect ratio (length/height) $A = 4$ has been considered as a benchmark at the GAMM Workshop (Roux, 1989), and since then has been investigated in detail (see for example Winters, 1988; Roux, 1989; Ben Hadid and Roux, 1989; Pulicani et al., 1989; Okada and Ozoe, 1993a, b; Afrid and Zebib, 1990; Gelfgat and Tanasawa, 1994; McClelland, 1995 and references therein). This particular value of the aspect ratio is characteristic for some crystal growth techniques and was used in the experiments of Hurle et al. (1974). However, the dependence of the steady-oscillatory transition on the aspect ratio of the cavity was not examined.

In the present study, the dependence of the critical parameters (critical Grashof number Gr_{cr} and critical frequency ω_{cr} of oscillations) on the aspect ratio is investigated for $1 \le A \le 10$, and for the following boundary conditions: rigid isothermal vertical boundaries, rigid adiabatic lower boundary, and flat stress-free adiabatic upper boundary. This corresponds to the Ra-Fa (**R**igid/**a**diabatic and stress-**F**ree/**a**diabatic horizontal boundaries) case defined at the GAMM workshop. Investigation is carried out for the same values of the Prandtl number Pr = 0 and 0.015, which were considered at the GAMM workshop (Roux, 1989). Stability diagrams for the whole interval $1 \le A \le 10$ are obtained here for the first time.

The stress-free upper boundary condition (denoted as R-F case in the GAMM workshop; Roux, 1989) was taken into consideration here because only one branch of steady-state flows is known for this case, at least for fluids with small Prandtl number (we consider here only Pr = 0 and 0.015). The case of cavity with four no-slip boundaries (R-R case) is more complicated for numerical study because of the existence of multiple stable steady states. The existence of two different steady states of the flow for $A = 4$ was reported by Crespo del Arco et al. (1989). Recently, Gelfgat, Bar-Yoseph and Yarin (1997) reported the existence of four distinct branches of stable-steady states for $3 \le A \le 10$. Besides this, the central symmetry of the flow in R-R case may cause symmetry-breaking instabilities which makes stability features of the flow in R-R and R-F cases considerably different. The stiff dependence of the critical parameters on the geometry of the cavity shown here allows us to assume that similar stiff dependence on the boundary conditions also exists.

Choice of the stress-free boundary condition on the upper surface is idealization of the practically important model which includes also the thermocapillary force (see for example Ben Hadid and Roux, 1989; Mundrane and Zebib, 1994) and possible deformation of the free surface (McClelland, 1995). However, calculation of the stability maps in the space of several governing parameters has to be started by fixing some of them. It is a natural choice to set the thermocapillary force and the deformation of the free surface to zero for the beginning of such study.

Setting the Prandtl number to zero means that the convective transport of heat is neglected. In this case the temperature can be evaluated analytically from the steady Laplace equation and only the Navier-Stokes equation with the constant buoyancy force has to be solved. This allows one to simplify the problem which may be important for many practical applications. The comparison of the steady-oscillatory transition at zero and small Prandtl numbers is one of the objectives of the present study. Another objective of the study is to check for which values of the aspect ratio it is possible to use the asymptotics of the infinite fluid layer ($A \to \infty$; Laure and Roux, 1989). If such an asymptotics could be applied to a confined flow, the investigation of the instability onset, as well as understanding of the physics of the phenomenon, will be simplified.

Formulation of the Problem

The two-dimensional convective flow in a rectangular cavity $0 \le x \le A$, $0 \le y \le 1$ is described by the dimensionless

Contributed by the Fluids Engineering Division for publication in the JOURNAL OF FLUIDS ENGINEERING. Manuscript received by the Fluids Engineering Division September 5, 1996; revised manuscript received June 23, 1997. Associate Technical Editor: Jong H. Kim.

momentum, energy and continuity equations for a Newtonian Boussinesq fluid

$$\frac{\partial \mathbf{v}}{\partial t} + (\mathbf{v}\cdot\nabla)\mathbf{v} = -\nabla p + \Delta\mathbf{v} + \mathrm{Gr}\theta\mathbf{e}_y, \qquad (1)$$

$$\frac{\partial \theta}{\partial t} + (\mathbf{v}\cdot\nabla)\theta = \frac{1}{\mathrm{Pr}}\Delta\theta, \quad \nabla\cdot\mathbf{v} = 0 \qquad (2, 3)$$

Here $\mathbf{v}$ is the fluid velocity, θ is the temperature, p is the pressure, $\mathrm{Gr} = g\beta(\theta_1 - \theta_2)H^3/\nu^2$ is the Grashof number, $\mathrm{Pr} = \nu/\chi$-is the Prandtl number, $A = L/H$ is the aspect ratio, g is the gravity acceleration, β is the thermal expansion coefficient, $(\theta_1 - \theta_2)$ is the temperature difference between the cold and hot vertical walls, ν is the kinematic viscosity, χ is the thermal diffusivity, L and H are, respectively, the length and the height of the cavity.

The following boundary conditions are imposed:

$$\mathbf{v}(x = 0, 0 \le y \le 1) = \mathbf{0}, \quad \mathbf{v}(x = A, 0 \le y \le 1) = \mathbf{0}$$

(no-slip; vertical walls), (4, 5)

$$\mathbf{v}(0 \le x \le A, y = 0) = \mathbf{0} \quad \text{(no-slip; bottom)}, \qquad (6)$$

$$v_y(0 \le x \le A, y = 1) = 0, \quad \frac{\partial v_x}{\partial y}(0 \le x \le A, y = 1) = 0,$$

(stress-free; flat upper surface) (7, 8)

$$\theta(x = 0, 0 \le y \le 1) = 1, \quad \theta(x = A, 0 \le y \le 1) = 0$$

(isothermal; vertical walls) (9)

$$\frac{\partial \theta}{\partial y}(0 \le x \le A, y = 0) = \frac{\partial \theta}{\partial y}(0 \le x \le A, y = 1) = 0$$

(thermally insulated top and bottom) (10, 11)

Computational Method

Problem (1)–(11) was solved using the spectral Galerkin method with globally defined basis functions which satisfy analytically all the boundary conditions and the continuity equation. The exponential convergence of the global Galerkin method allows us to decrease the number of degrees of freedom (number of scalar modes in the numerical method), and to investigate steady states, their stability and weakly supercritical regimes of the flow in the framework of a single computational model (for computational details and some preliminary test calculations see Gelfgat and Tanasawa (1994)). In particular, it was shown that for $A = 4$ use of 24 basis functions in horizontal and 10 basis functions in vertical directions provides accuracy comparable with the finite element method using 60×20 biquadratic finite elements (Winters, 1988) and the pseudospectral method with Chebyshev polynomial expansions using 50×20 collocation points (Pulicani et al., 1989).

The whole numerical process is as follows. Steady states of the flow are calculated by the Newton method. Then the Navier-Stokes equations are linearized in the vicinity of a stationary solution, and the corresponding spectrum and eigenmodes are calculated. The critical Grashof number is defined as the value at which the real part of the dominant eigenvalue is zero. The corresponding eigenvector describes the most unstable perturbation of the flow (the critical eigenmode). After the critical Grashof number is obtained, the weakly nonlinear analysis of the bifurcation is carried out. The slightly supercritical states of the flow are approximated as

$$\mathrm{Gr} = \mathrm{Gr}_{cr} + \mu\epsilon^2 + O(\epsilon^4),$$

$$T(\mathrm{Gr}) = \frac{2\pi}{\omega_{cr}}[1 + \tau\epsilon^2 + O(\epsilon^4)], \qquad (12, 13)$$

$$\{\mathbf{v}, \theta\}(t, \mathrm{Gr}) = \{\mathbf{v}_0, \theta_0\}(\mathrm{Gr}_{cr}) + \epsilon\,\mathrm{Real}\left[\{\mathbf{v}_E, \theta_E\}\exp\left(\frac{2\pi i}{T}\right)\right] + O(\epsilon^2) \qquad (14)$$

Here ϵ is a small formal parameter, T is the period of oscillations, ω_{cr} is the critical cycle frequency (the imaginary part of the dominant eigenvalue at $\mathrm{Gr} = \mathrm{Gr}_{cr}$). The subscript 0 defines the steady state at $\mathrm{Gr} = \mathrm{Gr}_{cr}$, and the subscript E defines the eigenvector of the linearized Boussinesq equations. The asymptotic approximation (12–14) of the oscillatory state is defined by two parameters μ and τ, which are calculated using the algorithm described in Hassard et al. (1981). Application of this algorithm to the dynamic system corresponding to an incompressible fluid flow is described in Gelfgat et al. (1996a).

The convergence of the critical Grashof number and the critical frequency ($f_{cr} = \omega_{cr}/2\pi$) is shown in the Table 1 for the aspect ratios 1, 4, and 10, respectively. Grashof number in Tables 1–3 is redefined as $\mathrm{Gr}^* = \mathrm{Gr}/A$ in according with the definitions used in the GAMM benchmark problem (Roux, 1989). The critical parameters were calculated using different number of basis functions in the Galerkin series. Numbers of basis functions in x- and y-directions are denoted as N_x and N_y, respectively. It follows from Table 1 that for $A = 1$ and 4 the critical parameters Gr^*_{cr} and f_{cr} converge rapidly with the increase of the number of basis functions. As it is seen from the Table 1 the convergence for $A = 10$ is slower, but two correct digits of Gr_{cr} and f_{cr} can be obtained with the use of 60×20 basis functions.

The numerical code has been validated by comparing its results with other independent solutions (Tables 2 and 3). It is seen (Table 2) that the present results, obtained using the stability analysis, are in a good agreement (to within the second or the third digit) with the results of Ben Hadid and Roux (1989), Pulicani et al. (1990), Le Quere (1989), and Winters (1988). The discrepancy with the results of Okada and Ozoe (1993) is about 10 percent. An additional comparison with the results of the same work for other aspect ratios is shown in Table 3. For $A = 3$, 4 and 5 the discrepancy is also about 10 percent, but at $A = 2.5$ results disagree completely. Since the result of the present work for $A = 4$ is completely validated (see Table 1) and is compared better with the results of other numerical studies, it seems that the results of this reference are not accurate enough.

To ensure convergence, the present calculations were carried out using 40×30 basis functions for $1 \le A \le 5$ and 60×20 basis functions for $4 \le A \le 10$. In the interval $4 \le A \le 5$ the results obtained with the two different truncations coincide to within the third digit.

Results

Numerical investigation of the spectrum of the steady states showed that for the two considered values of the Prandtl number, $\mathrm{Pr} = 0$ and 0.015, and for the whole interval $1 \le A \le 10$ the oscillatory instability sets in due to the Hopf bifurcation.

The dependence of the critical Grashof number Gr_{cr} on the aspect ratio is shown in Figs. 1(a) and 2(a) for $1 \le A \le 3$ and $3 \le A \le 10$, respectively. Steady flows are stable below the curves and unstable above them. The corresponding relations $\omega_{cr}(A)$ are shown in Figs. 1(b) and 2(b). As it is seen from Figs. 1 and 2 the curves $\mathrm{Gr}_{cr}(A)$ and $\omega_{cr}(A)$ consist of several continuous branches corresponding to different dominant perturbations (different eigenmodes of the linearized problem). These eigenmodes become dominant at different values of the aspect ratio and abruptly replace each other at the points where the neutral curves $\mathrm{Gr}_{cr}(A)$ have discontinuities in the slope (Figs. 1(a) and 2(a)). Switches of the dominant eigenmode lead to abrupt changes of the critical frequency (Figs. 1(b) and 2(b)).

Table 1 Convergence study for the critical parameters. $Gr^*_{cr} = Gr/A$, N_x and N_y denote number of basis functions respectively in x- and y- directions

			$A = 1$			
$N_x \times N_y$	16 × 16	20 × 20	26 × 26	30 × 30	36 × 36	40 × 40
$Gr^*_{cr} \times 10^{-6}$	2.6956	2.6776	2.7695	2.7471	2.7467	2.7467
f_{cr}	1474.8	1458.8	1469.4	1466.5	1466.4	1466.4
			$A = 4$			
$N_x \times N_y$	32 × 18	36 × 22	40 × 26	50 × 20	40 × 30	60 × 24
Gr^*_{cr}	19404	19403	19380	19361	19363	19363
f_{cr}	14.916	14.915	14.909	14.901	14.903	14.901
			$A = 10$			
$N_x \times N_y$	40 × 18	50 × 20	70 × 20	60 × 20	66 × 24	70 × 24
Gr^*_{cr}	61917	62314	61942	61663	62330	62515
f_{cr}	51.17	51.30	51.13	50.98	51.34	51.48

Figures 1 and 2 show that the functions $Gr_{cr}(A)$ and $\omega_{cr}(A)$ are non-monotone and very sensitive to a small change of the aspect ratio or the Prandtl number. For example, at Pr = 0.015 the values of the critical Grashof number and the critical frequency for $A = 1.7$ and $A = 1.8$ differ drastically (Fig. 1). The difference between the critical parameters at Pr = 0.015 and Pr = 0 is relatively large almost everywhere except in the interval $3 \le A \le 4.95$ (Figs. 2(a) and (b)). Such a big difference in critical parameters for zero and small values of the Prandtl number means that the convective heat transfer plays a significant role in the onset of instability and cannot be neglected when stability features of the flow are considered. This leads to the conclusion that extrapolation of results, obtained for particular values of the Prandtl number or the aspect ratio, to other, even very close, values of the control parameters should be done with an extreme caution.

It is seen from Fig. 2(a) that the function $Gr_{cr}(A)$ has a global minimum very close to $A = 4$. This value of the aspect ratio was chosen for a comparative study with the benchmark of the GAMM workshop (Roux, 1989). Note that this particular value of the aspect ratio may not be a very good choice, since calculations for smaller values of Gr are always more accurate than for larger ones. Moreover, in the interval $3 \le A \le 4.95$, the onset of instability for Pr = 0.015 and Pr = 0 is similar (see Fig. 4) and investigation of only a single value of the aspect ratio may lead to a wrong conclusion that the convective heat transfer can be neglected (see Gelfgat and Tanasawa, 1994 for $A = 4$).

There are two hysteresis loops of the critical Grashof number for Pr = 0.015. One is located near $A = 1.6$ (Fig. 1(a)), and another one is located in the interval $4.9 \le A \le 5$ (Fig. 2(a)). The hysteresis of Gr_{cr} means that there are three critical values $Gr^1_{cr} < Gr^2_{cr} < Gr^3_{cr}$. The first steady-oscillatory transition occurs at $Gr = Gr^1_{cr}$. With the increase of Gr a backwards transition from an oscillatory to a stable steady state takes place at $Gr = Gr^2_{cr}$, and then, at $Gr = Gr^3_{cr}$, the steady flow finally bifurcates to the oscillatory state. Each of the three transitions is characterized by its critical frequency such that in the hysteresis regions there are 3 critical frequencies corresponding to a single value of the aspect ratio (magnified areas in Figs. 1(b) and 2(b)).

The first hysteresis (Fig. 1(a)) takes place on the branch of the neutral curve which starts at $A \approx 1.59$ (point I in Fig. 1(a)), continues with the decrease of A and Gr_{cr} up to $A \approx 1.57$ (point II), and with the increase of A and Gr_{cr} ends at $A \approx 1.69$ (point III). For example, at $A = 1.59$ the first steady-oscillatory transition takes place at $Gr^1_{cr} = 1.17 \times 10^6$, then the oscillatory-steady transition at $Gr^2_{cr} = 1.63 \times 10^6$, and the final steady-oscillatory transition at $Gr^3_{cr} = 1.77 \times 10^6$ (which belongs to the previous branch of the neutral curve).

The second hysteresis loop (Fig. 2(a)) starts at $A \approx 4.93$ (point IV in Fig. 2(a)) where the neutral curve turns such that the critical Grashof continues to grow with the decrease of the

Table 2 Comparison with the published results ($A = 4$, Pr = 0, $Gr^*_{cr} = Gr/A$)

Reference	Discretization	Gr^*_{cr}	f_{cr}
Okada and Ozoe (1993)	121 × 35 finite difference non-uniform grid	15050	13.08
Ben Hadid and Roux (1989)	121 × 41 finite difference non-uniform grid	13500–13750	12.25–12.42
Pulicani et al (1990)	27 × 15 Chebyshev spectral modes	13100–13500	12.32–12.37
Le Quere (1989)	50 × 20 Chebyshev pseudospectral modes	13650	12.33
Winters (1988)	60 × 24 biquadratic finite elements (121 × 49 non-uniform grid)	13722	12.36
Present work	40 × 30 spectral modes	13683	12.34

Table 3 Comparison with the results of Okada and Ozoe, 1993a (Pr = 0, $Gr^*_{cr} = Gr/A$)

	Okada and Ozoe (1993)			Present work		
A	Mesh	Gr^*_{cr}	f_{cr}	Number of basis functions	Gr^*_{cr}	f_{cr}
2.5	85 × 35	90490	60.86	40 × 30	63916	45.12
3	121 × 41	30170	22.05	40 × 30	26703	20.39
4	121 × 35	15050	13.08	40 × 30	13683	12.34
5	151 × 35	13220	12.03	50 × 20	12136	11.31

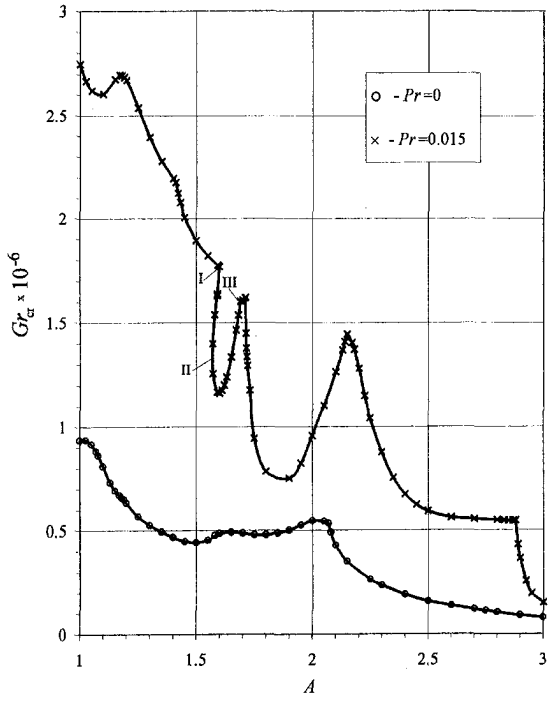

Fig. 1(*a*) Dependence $Gr_{cr}(A)$

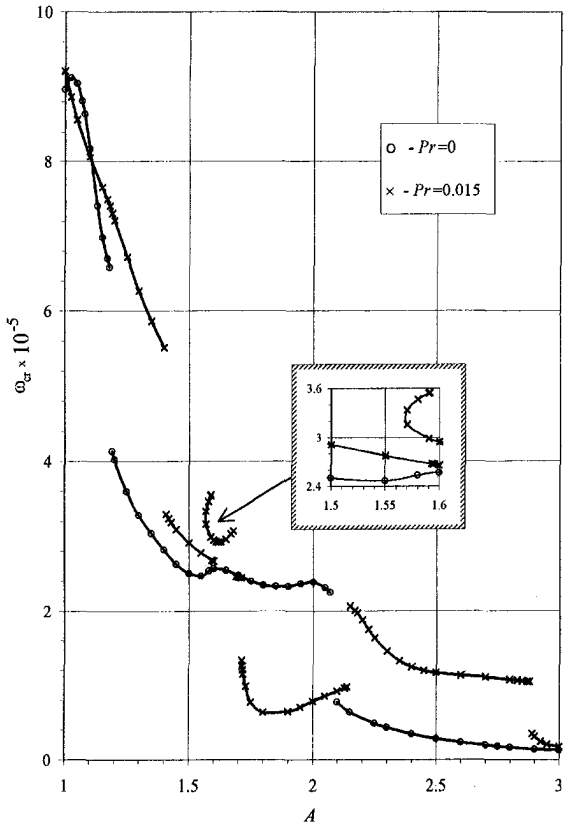

Fig. 1(*b*) Dependence $\omega_{cr}(A)$

Fig. 1 Stability diagram for aspect ratio $1 \leq A \leq 3$.

aspect ratio. When the aspect ratio reaches the value $A \approx 4.85$ (point V) the neutral curve turns once more such that Gr_{cr} increases with the increase of A, e.g. at $A = 4.9$ three critical values of the Grashof number are 1.09×10^5, 1.45×10^5, and 1.88×10^5.

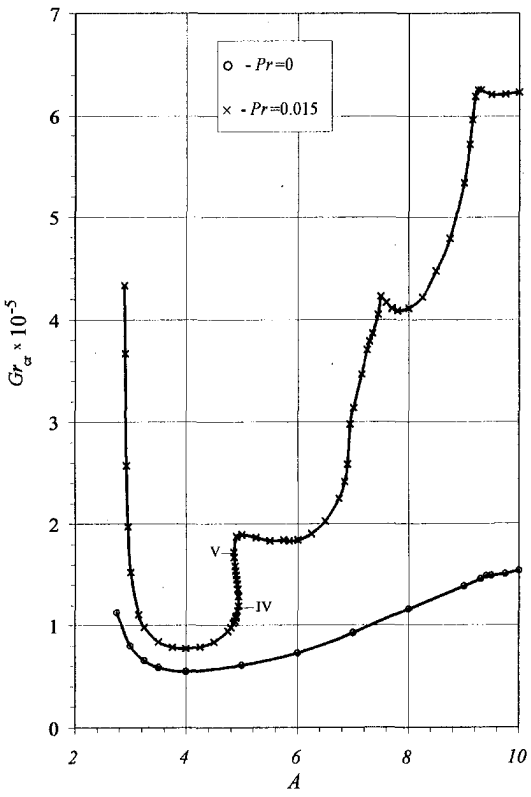

Fig. 2(*a*) Dependence $Gr_{cr}(A)$

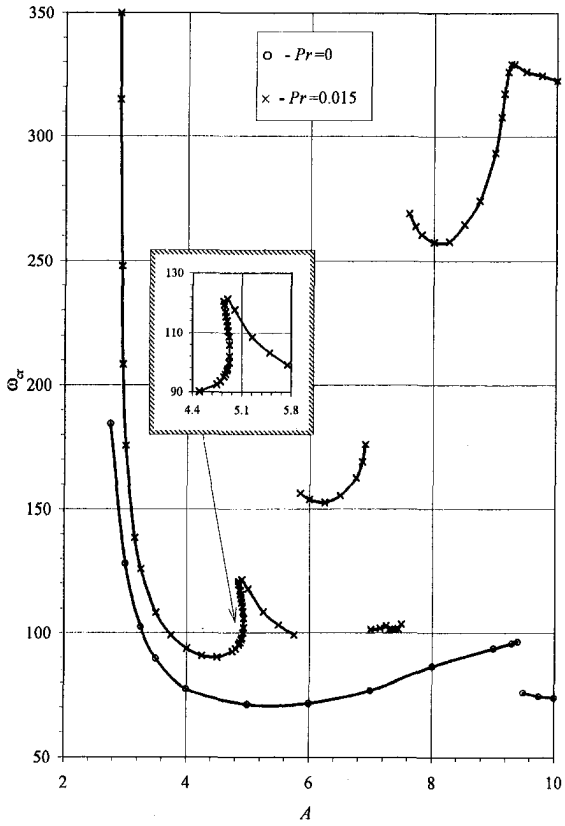

Fig. 2(*b*) Dependence $\omega_{cr}(A)$

Fig. 2 Stability diagram for aspect ratio $3 \leq A \leq 10$.

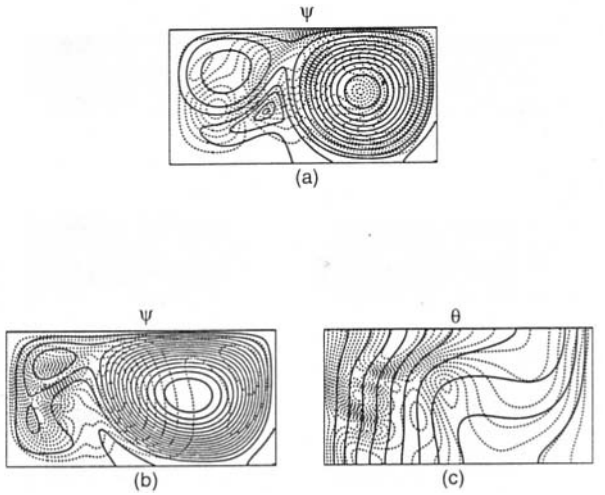

Fig. 3 Isolines of the stream function and the temperature (solid lines), and the corresponding dominant perturbations (dashed lines) for aspect ratio $A = 2$. All isolines, except the stream lines $\psi \leq 0$, are equally spaced. (*a*) Pr = 0, $Gr_{cr} = 5.47 \times 10^5$; $\psi_{max} = 502.9$, $\psi_{min} = -8.957$, (*b*) Pr = 0.015, $Gr_{cr} = 9.59 \times 10^5$; $\psi_{max} = 318.5$, $\psi_{min} = -2.135$.

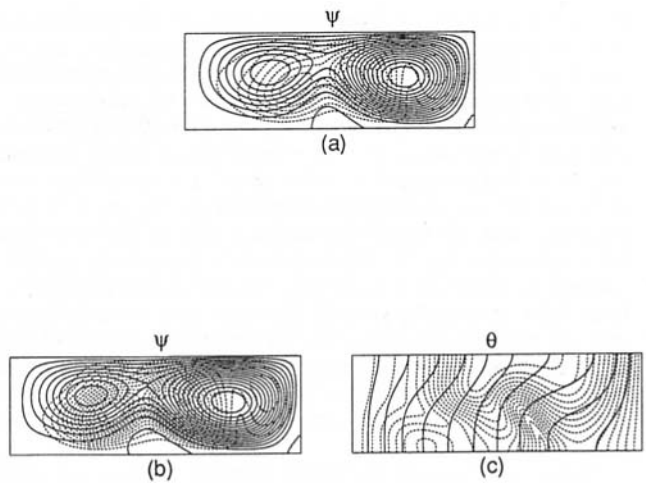

Fig. 4 Isolines of the stream function and the temperature (solid lines), and the corresponding dominant perturbations (dashed lines) for aspect ratio $A = 3$. All isolines, except the stream line $\psi = 0$, are equally spaced. (*a*) Pr = 0, $Gr_{cr} = 8.01 \times 10^4$; $\psi_{max} = 104.8$, $\psi_{min} = -0.5194$, (*b*) Pr = 0.015, $Gr_{cr} = 1.54 \times 10^5$; $\psi_{max} = 141.6$, $\psi_{min} = -0.8440$.

To compare the results with the case of an infinite fluid layer it is necessary to redefine the Grashof number using the average temperature gradient $(\theta_1 - \theta_2)/L$ instead of the characteristic temperature difference $(\theta_1 - \theta_2)$. This yields $Gr^* = g\beta(\theta_1 - \theta_2)H^4/L\nu^2 = Gr/A$. Figure 2 shows that no well defined asymptotic behavior is reached for Gr (neither for Gr*) at aspect ratios close to $A = 10$. Moreover, there is a switch of the dominant perturbation in the interval $9 \leq A \leq 10$ for both values of the Prandtl number Pr = 0 and 0.015 (Fig. 2). Further investigation is necessary to find for which values of A, the infinite layer solution is a valid approximation.

Examples of steady flows at critical values of parameters and the corresponding dominant perturbations are shown in Figs. 3–5 for $A = 2$, 3 and 8. Flows and perturbations for $A = 1$, 4, and 10 are described in Gelfgat and Tanasawa (1994) and Gelfgat et al. (1996b). Since the eigenvector of the linearized problem is a complex vector (see Eq. (14)) which is defined within multiplication by a complex constant, its modulus is used to describe the dominant perturbations. Note that for slightly supercritical oscillatory flows the isolines of the amplitude of oscillations coincide with the isolines of modulus of the perturbation. Each plot in Figs. 3–5 is arranged in the following way: solid curves show isolines of the stream function ψ and the temperature θ. Dashed lines show isolines of the modulus of the most dominant perturbations of functions ψ and θ. For Pr = 0 only the stream function and its perturbation are reported.

In the case Pr = 0 the buoyancy force is constant and the temperature is not perturbed at all. This means that only the fluid flow itself can become unstable, i.e., the instability is caused by the hydrodynamic effect only (heat transfer does not influence the flow stability). This instability is called hydrodynamic instability to distinguish it from the other possible types of instability, which may arise at non-zero Prandtl numbers and may be caused by a thermal-hydrodynamic effect.

Flow patterns and their corresponding dominant perturbations for $A = 2$ are shown in Fig. 3. It is seen that the perturbations of the stream function for Pr = 0 (Fig. 3(*a*)) and Pr = 0.015 (Fig. 3(*b*)) are different: the perturbation of ψ at Pr = 0 has a global maximum in the center of the main convective vortex, while at Pr = 0.015 maximal values of the perturbation of ψ are located near the hot wall. This difference in the patterns means that the onset of the instability at Pr = 0.015 is influenced by the thermal effects and differs from those at Pr = 0. The perturbation of θ (Fig. 3(*c*)) also has a global maximum near the hot wall. This allows us to conclude that the oscillatory instability initiates in the form of oscillations of the velocity and the temperature near the hot wall where convective flow and convective heat transfer are relatively weak (see isolines of ψ and θ in Fig. 3(*b*) and (*c*)).

Figure 4 corresponds to the case $A = 3$ for which the oscillatory instability at Pr = 0 (Fig. 4(*a*)) and Pr = 0.015 (Fig. 4(*b*)) is of the same hydrodynamic type. This conclusion follows from the similarity of the patterns of the perturbations of ψ for two values of the Prandtl number (Fig. 4(*a*) and 4(*b*)). According to the results of this study (Fig. 2), this similarity is preserved only in the interval $3 \leq A \leq 4.95$ (for the case $A = 4$ see Gelfgat and Tanasawa (1994) and Gelfgat et al. (1996b)).

Results for a larger aspect ratio, $A = 8$, are plotted in Fig. 5. Note that at Pr = 0 the critical points for $A = 3$ and $A = 8$ belong to the same branch of the neutral curve, and to different branches at Pr = 0.015 (Fig. 2). Comparison of Figs. 4 and 5 shows that at Pr = 0 the maximum of the perturbation of ψ is located at the outer boundary of the strongest meridional circulation both for $A = 3$ and 8. The same was observed for $A = 4$ (see Gelfgat and Tanasawa, 1994 and Gelfgat et al., 1996b). The pattern of the perturbation at Pr = 0.015 is different

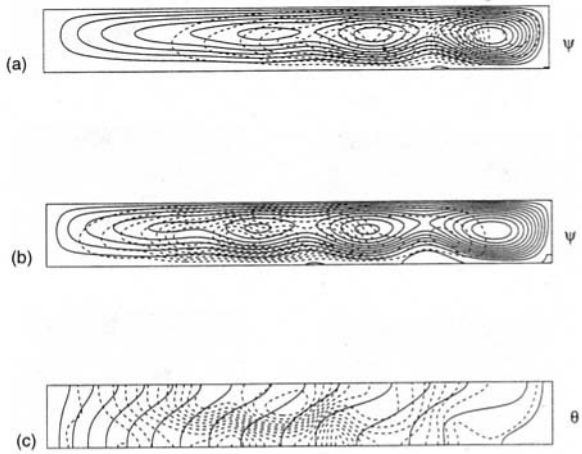

Fig. 5 Isolines of the stream function and the temperature (solid lines), and the corresponding dominant perturbations (dashed lines) for aspect ratio $A = 8$. All isolines, except the stream line $\psi = 0$, are equally spaced. (*a*) Pr = 0, $Gr_{cr} = 1.16 \times 10^5$; $\psi_{max} = 94.79$, $\psi_{min} = -0.009570$, (*b*) Pr = 0.015, $Gr_{cr} = 4.11 \times 10^5$; $\psi_{max} = 209.9$, $\psi_{min} = -2.651$.

(Figs. 5(*b*) and 5(*c*)). Two local maxima of the perturbation of ψ are located near weaker meridional circulations, and the global maximum of the perturbation of θ is located in the same area. As it was previously reported for $A = 10$ (Gelfgat et al., 1996b) and for both cases, Pr = 0 and Pr = 0.015, the flow and their perturbations do not contain any spatially periodic structures. With the increase of the aspect ratio, the global maximum of the stream function remains near the cold vertical boundary, and the whole convective vortex is shifted toward the colder area (Fig. 5). This means that no spatially periodic structure is observed. It is obvious that the dominant perturbation of the nonspatially-periodic flow also does not contain any spatially periodic structures. So, the asymptotic case of an infinite fluid layer ($A \to \infty$) cannot be applied for the considered finite aspect ratio cases ($A \leq 10$). Significantly larger values of the aspect ratio must be considered for investigation of this asymptotic behavior.

Slightly supercritical oscillatory states of the flow are illustrated in Figs. 6–8 for $A = 2$, 3 and 8, respectively. The oscillatory states were approximated asymptotically using weakly nonlinear analysis of the Hopf bifurcation (Hassard et al., 1981) which results in Eqs. (12)–(14). All the supercritical states were approximated for 10 percent supercriticality.

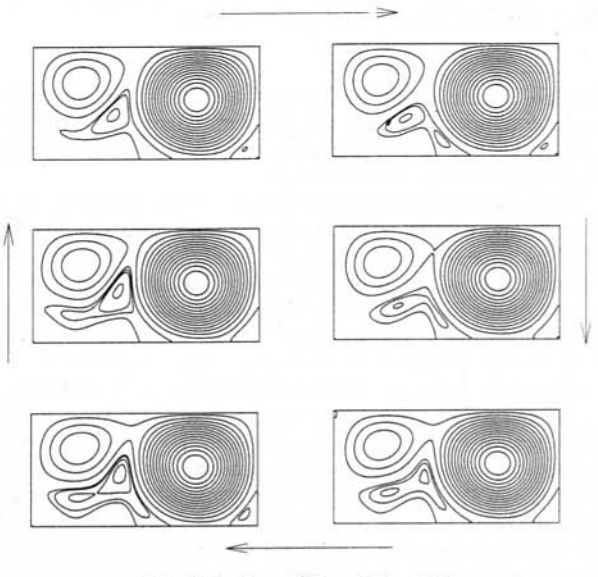

Fig. 6(*a*) Pr = 0, Gr = 5.65×10^5

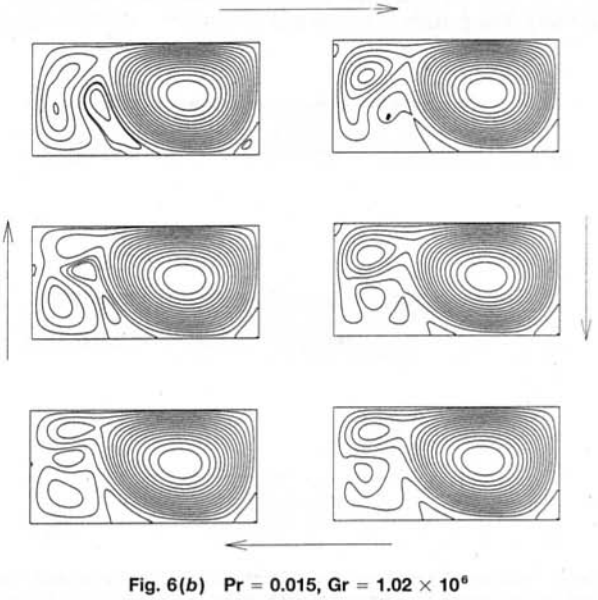

Fig. 6(*b*) Pr = 0.015, Gr = 1.02×10^6

Fig. 6 Instantaneous streamlines of the convective flow plotted for equal time intervals *T*/6 covering the complete period. Aspect ratio *A* = 2.

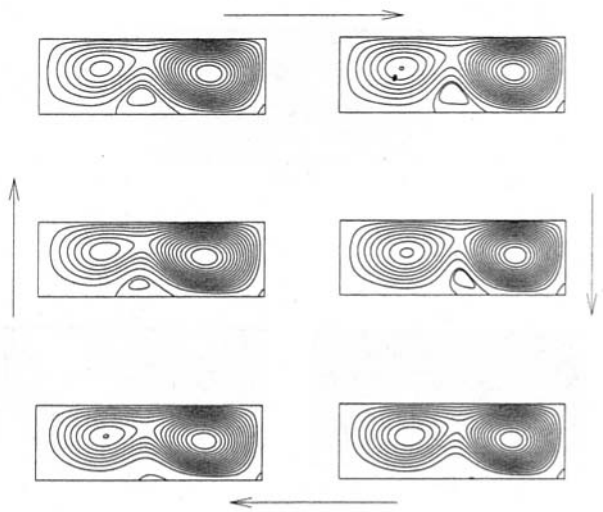

Fig. 7 Instantaneous streamlines of the convective flow plotted for equal time intervals *T*/6 covering the complete period. Aspect ratio *A* = 3. Pr = 0, Gr = 8.8×10^4.

Figure 6 shows the slightly supercritical states for Pr = 0 and 0.015 in a cavity with $A = 2$. One can see that the onset of instability due to different dominant perturbations leads to different oscillations in time. Thus at Pr = 0 perturbation of the stream function has a global maximum inside the main convective circulation (Fig. 3(*a*)). This leads to oscillations of the two clockwise circulations (the stronger and the weaker ones) which merge and split during one period of oscillations (Fig. 6(*a*)). This is followed by oscillations of a weak reverse vortex attached to the lower boundary. Oscillations at Pr = 0.015 are different. Perturbations of the stream function and the temperature in this case are located near the hot wall where the convective motion is relatively weak (Figs. 3(*b*) and 3(*c*)). According to this, oscillations of the stream function, shown in Fig. 6(*b*) have larger amplitude near the hot wall. The main circulation, shifted toward the cold wall, remains almost undeformable during the period of oscillations.

Slightly supercritical oscillatory flow at $A = 3$ and Pr = 0 is shown in Fig. 7. Perturbations for Pr = 0 and 0.015 are similar for this aspect ratio, so the oscillations in slightly supercritical states look similarly. The oscillations appear as weak pulsations of the two local maxima of the stream function followed by oscillations of a weak reverse vortex attached to the lower boundary. This asymptotically approximated oscillatory flow is similar to the flow calculated for $A = 4$ (Gelfgat et al., 1996b), and is in qualitative agreement with the results of the direct numerical solution of the full unsteady problem (Roux, 1989; Pulicani et al., 1989).

Figure 8 illustrates a slightly supercritical oscillatory flows at $A = 8$. At Pr = 0 the critical Grashof numbers for $A = 3$ and 8 belong to the same branch of the neutral curve (Fig. 2). So, the perturbations and the oscillations in both cases are similar (compare Figs. 4(*a*) and 5(*a*) to Figs. 7(*a*) and 8(*a*). At $A = 8$ (Pr = 0, Fig. 8(*a*)) one can see oscillations of the clockwise meridional circulations followed by oscillations of two weak counter clockwise vortices attached to the lower wall. In the case Pr = 0.015 perturbations of ψ and θ are located in the central part of the cavity (Figs. 5(*b*) and 5(*c*)). Accordingly, oscillations of the stream function have larger amplitudes in the central part of the cavity (Fig. 8(*b*)), where one can see oscillations of several clockwise circulations. Oscillations of the weak counter clockwise vortices are much weaker than in the case Pr = 0.

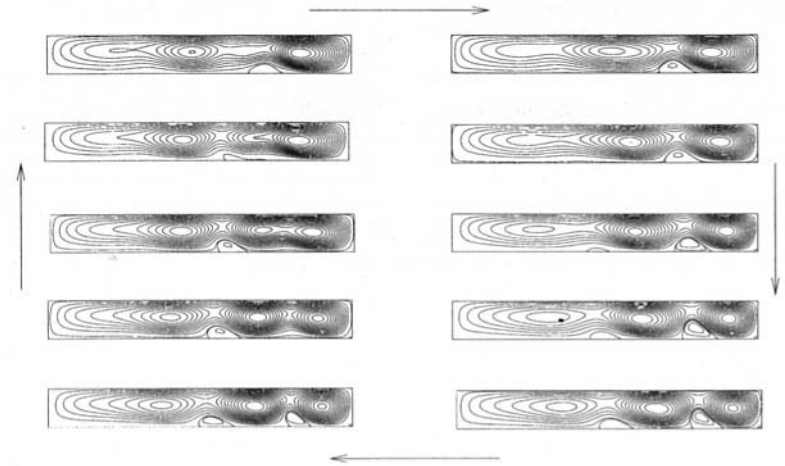

Fig. 8(*a*) Pr = 0, Gr = 1.3×10^5

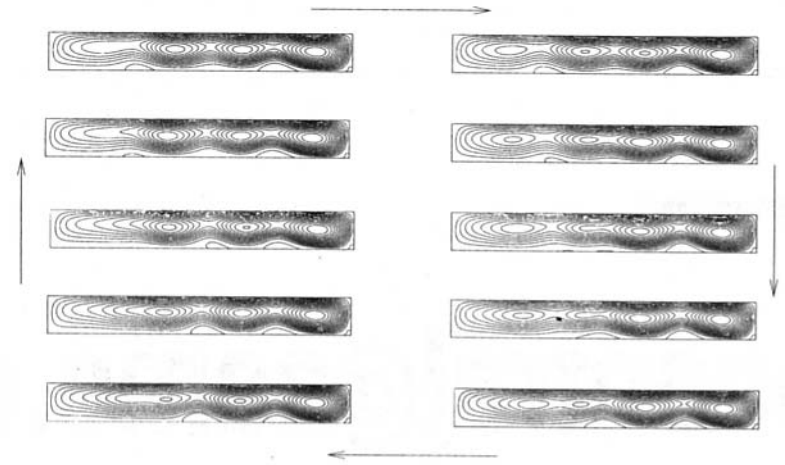

Fig. 8(*b*) Pr = 0.015, Gr = 4.5×10^5

Fig. 8 Instantaneous streamlines of the convective flow plotted for equal time intervals *T*/6 covering the complete period. Aspect ratio *A* = 8.

Conclusions

The oscillatory instability of the considered convective flow sets in due to Hopf bifurcation in the whole interval $1 \leq A \leq 10$ and for the considered values of the Prandtl number (Pr = 0 and 0.015). The dependence of the critical parameters (critical Grashof number and the frequency of oscillations) on the aspect ratio and the Prandtl number is very complicated, and very sensitive to a small change of the control parameter. Stability diagrams show that using the stability features for predicting of other (even close) values of the control parameter is not always possible. In particular, the convective heat transfer is not negligible even at low-Prandtl-number (like Pr = 0.015) flows.

The results for the asymptotic limit of an infinite fluid layer ($A \to \infty$) cannot be used even for long horizontal cavities with the aspect ratio up to $A = 10$. This means that in practically important situations, the finite dimension of the cavity and the corresponding end effects should always be taken into account.

Acknowledgment

This research was supported by the German-Israeli Foundation for Scientific Research and Development, grant No. I-284.046.10/93.

References

Afrid M., and Zebib A. 1990. "Oscillatory Three-Dimensional Convection in Rectangular Cavities and Enclosures," *Physics of Fluids A,* Vol. 2(8), pp. 1318–1327.

Ben Hadid H, and Roux B. 1989a. "Buoyancy and Thermocapillary-Driven Flows in a Shallow Cavity: Unsteady Flow Regimes," *Journal of Crystal Growth,* Vol. 97, pp. 217–225.

Ben Hadid H, and Roux B. 1989b. "Buoyancy-Driven Oscillatory Flows in Shallow cavities Filled with Low-Prandtl Number Fluids," *Proc. GAMM Workshop on Numerical Solution of Oscillatory Convection in Low Prandtl Number Fluids* (ed., B. Roux), Marseille, 1988, Notes on Numerical Fluid Mechanics, Vieweg Braunschweig, Vol. 27, pp. 25–33.

Gelfgat A. Yu., and Tanasawa I., 1994, "Numerical Analysis of Oscillatory Instability of Buoyancy Convection with the Galerkin Spectral Method," *Numerical Heat Transfer,* Part A, Vol. 25, pp. 627–648.

Gelfgat A. Yu., Bar-Yoseph P. Z., and Solan A., 1996a, "Stability of a Confined Swirling Flows with and without Vortex Breakdown," *Journal of Fluid Mechanics,* Vol. 311, pp. 1–36.

Gelfgat A. Yu., Bar-Yoseph P. Z., and Yarin A., 1996b, "Numerical Investigation of Hopf Bifurcation Corresponding to transition from Steady to oscillatory State in a Confined Convective flow," *Proc. 1996 Fluids Engineering Division Conference,* San-Diego, CA, July 7–11, Vol. 2, FED-Vol. 237, pp. 369–374.

Gelfgat A. Yu., Bar-Yoseph P. Z., and Yarin A., 1997. "Patterns of Bifurcating Convective Flows in Long Horizontal Cavities," *Advances in Computational Heat Transfer* (ed. G. de Vahl Davis) to appear.

Hassard B. D., Kazarinoff N. D., and Wan Y.-H., 1981, "Theory and Applications of Hopf Bifurcation," London Mathematical Society Lecture Note Series, Vol. 41.

Hurle D. T. J., Jakeman E., and Johnson C. P., 1974, "Convective Temperature Oscillations in Molten Gallium," *Journal of Fluid Mechanics,* Vol. 64, pp. 565–576.

Laure P., and Roux B., 1989, "Linear and Non-Linear Analysis of the Hadley Circulation," *Journal of Crystal Growth,* Vol. 97, pp. 226–234.

Le Quere P. 1989. "Contribution to GAMM Workshop with a Pseudo-Spectral Algorithm on a Staggered Grid," *Proc. GAMM Workshop on Numerical Solution of Oscillatory Convection in Low Prandtl Number Fluids* (ed. B. Roux). Marseille, 1988, Notes on Numerical Fluid Mechanics, Vieweg Braunschweig, Vol. 27, pp. 227–236.

McClelland M. A. 1995. "Time-Dependent Liquid Metal Flows with Free Convection and a Deformable Free Surface," *International Journal for Numerical Methods in Fluids,* Vol. 20, pp. 603–620.

Mundrane M, and Zebib A. 1994, "Oscillatory Buoyant Thermocapillary Flow," *Physics of Fluids,* Vol. 6(10), pp. 3294–3305.

Okada K., and Ozoe H. 1993a. "The Effect of Aspect Ratio on the Critical Grashof Number for Oscillatory Natural Convection of Zero Prandtl Number Fluid; Numerical Approach," *Journal of Crystal Growth,* Vol. 126, pp. 330–334.

Okada K., and Ozoe H. 1993b. "Various Computational Conditions of Oscillatory Natural Convection of Zero Prandtl Number Fluid in an Open Boat Heated and Cooled From Opposing Vertical Walls," *Numerical Heat Transfer,* Part A, Vol. 23, pp. 171–187.

Pulicani J. P., Crespo del Arco A., Randriampianina A. Bontoux P., and Peyret R., 1990, "Spectral Simulations of Oscillatory Convection at Low Prandtl Number," *International Journal for Numerical Methods in Fluids,* Vol. 10, pp. 481–517.

Roux B. (ed.), 1989, Proc. GAMM Workshop on Numerical Solution of Oscillatory Convection in Low Prandtl Number Fluids. Marseille, 1988," *Notes on Numerical Fluid Mechanics,* Vieweg Braunschweig, Vol. 27.

Winters K. H., 1988, "Oscillatory Convection in Liquid metals in a Horizontal Temperature Gradient," *International Journal of Numerical Methods in Engineering,* Vol. 25, pp. 401–414.